Oxygen Reduction Reaction

DOI: 10.1002/ange.201308896

Highly Efficient Electrocatalysts for Oxygen Reduction Based on 2D Covalent Organic Polymers Complexed with Non-precious Metals**

Zhonghua Xiang, Yuhua Xue, Dapeng Cao, Ling Huang, Jian-Feng Chen, and Liming Dai**

Abstract: *A class of 2D covalent organic polymers (COPs) incorporating a metal (such as Fe, Co, Mn) with precisely controlled locations of nitrogen heteroatoms and holes were synthesized from various N-containing metal–organic complexes (for example, metal–porphyrin complexes) by a nickel-catalyzed Yamamoto reaction. Subsequent carbonization of the metal-incorporated COPs led to the formation of COP-derived graphene analogues, which acted as efficient electrocatalysts for oxygen reduction in both alkaline and acid media with a good stability and free from any methanol-crossover/CO-poisoning effects.*

Platinum has been long known as the most effective catalyst for the oxygen reduction reaction (ORR) in fuel cells.[1] However, the scarcity, high cost, and poor long-term stability of the Pt-based ORR catalysts are main obstacles for commercialization of the fuel cell technology. Recently, Pt-based alloys and non-precious metals have been extensively studied as ORR electrocatalysts to reduce/replace the expensive Pt-based electrode in fuel cells. In particular, the development of carbon-supported transition metal/nitrogen (M-N_x/C) materials (M = Co, Fe, Ni, Mn, typically $x = 2$ or 4) as ORR electrocatalysts has attracted increasing attention since cobalt phthalocyanine was reported as the ORR electrocatalyst in alkaline electrolytes in 1964.[2] However, the ORR electrocatalysts based on cobalt phthalocyanine often show poor stability in acidic media owing to the fact that the coordinating bond between cobalt and nitrogen is susceptible to acid-induced decomposition.[3] To overcome this obstacle, subsequent high temperature treatment (ca. 400–1000 °C) was performed and some significant progresses have been achieved within the past decade.[2a]

Along with the recent intensive research efforts in the carbon-supported transition-metal ORR electrocatalysts, the recent discovery that heteroatom-doped graphitic carbon materials can act as efficient metal-free ORR electrocatalysts has attracted tremendous interest.[4] A large variety of heteroatom-doped carbon materials, including vertically aligned nitrogen-containing carbon nanotubes (VA-NCNTs),[5] N-doped graphene,[4a] B-doped carbon nanotubes,[4h] graphitic carbon nitride,[4i] and N-doped ordered mesoporous graphitic arrays,[6] have been demonstrated to act as metal-free ORR electrocatalysts by a four-electron process free from CO poisoning with a similar, or even higher, electrocatalytic activity and better long-term operation stability than that of commercially available Pt-based electrodes (for example, C2-20, 20% platinum on Vulcan XC-72R; E-TEK) in alkaline electrolytes. However, the ORR performance for many of the metal-free carbon-based electrocatalysts in acid media needs to be further improved to be competitive with the commercially available Pt-based electrodes.

We have recently synthesized a class of 2D covalent organic polymers (COPs) with precisely controlled locations of N heteroatoms and holes from various N-containing organic complexes (such as triazine, porphyrin, and their derivatives) by a nickel-catalyzed Yamamoto reaction.[7] The resultant COPs with high porosities are insoluble in common solvents and stable in acid and base media. Through complexation of non-noble metals (Fe, Co, Mn) with the porphyrin monomers for the Yamamoto polycondensation (Scheme 1), metal-incorporated COPs were produced, which could be further carbonized into C-COP materials with a rather uniform metal/nitrogen distribution and good stability in both alkaline and acid media. These materials show great potential for ORR applications; in particular, the Fe-incorporated C-COP exhibited a similar onset potential as that of the benchmarked Pt/C in both alkaline and acid media, while the Co-incorporated C-COP displayed an even higher kinetic current and diffusion-limiting current than those of the benchmarked Pt/C in alkaline solution (see below).

As shown in Scheme 1, we first introduced the metal (Fe, Co, or Mn) into monomers by metal–porphyrin complexation. Specifically, metal chloride and 5,10,15,20-tetrakis(4′-bromo biphenyl) porphine (TBBPP) were used to produce the metal-incorporated monomers: PF-M (M = Fe, Co, or Mn). As expected, the resultant PF-Fe, PF-Co, and PF-Mn showed characteristic peaks at $m/z = 1290.4$, 1289.3, and 1293.0, respectively, in the ESI-MS spectra recorded under the positive mode (Supporting Information, Figures S1–S3). The successful metal incorporation into TBBPP was further confirmed by the absence of the N-H peak characteristic of

[*] Dr. Z. Xiang, Dr. Y. Xue, Prof. L. Dai
Centre of Advanced Science and Engineering for Carbon (Case4-Carbon)
Department of Macromolecular Science and Engineering
Case Western Reserve University
10900 Euclid Avenue, Cleveland, OH 44106 (USA)
E-mail: liming.dai@case.edu
Dr. Z. Xiang, Prof. D. Cao, L. Huang, Prof. J.-F. Chen
State Key Lab of Organic–Inorganic Composites
Beijing University of Chemical Technology
Beijing 100029 (P.R. China)
E-mail: caodp@mail.buct.edu.cn

[**] This work was supported financially by State Key Lab of Organic-Inorganic Composites at BUCT, AFOSR (FA9550-12-1-0037), and NSF (IIP-134270).

Supporting information for this article is available on the WWW under http://dx.doi.org/10.1002/anie.201308896.

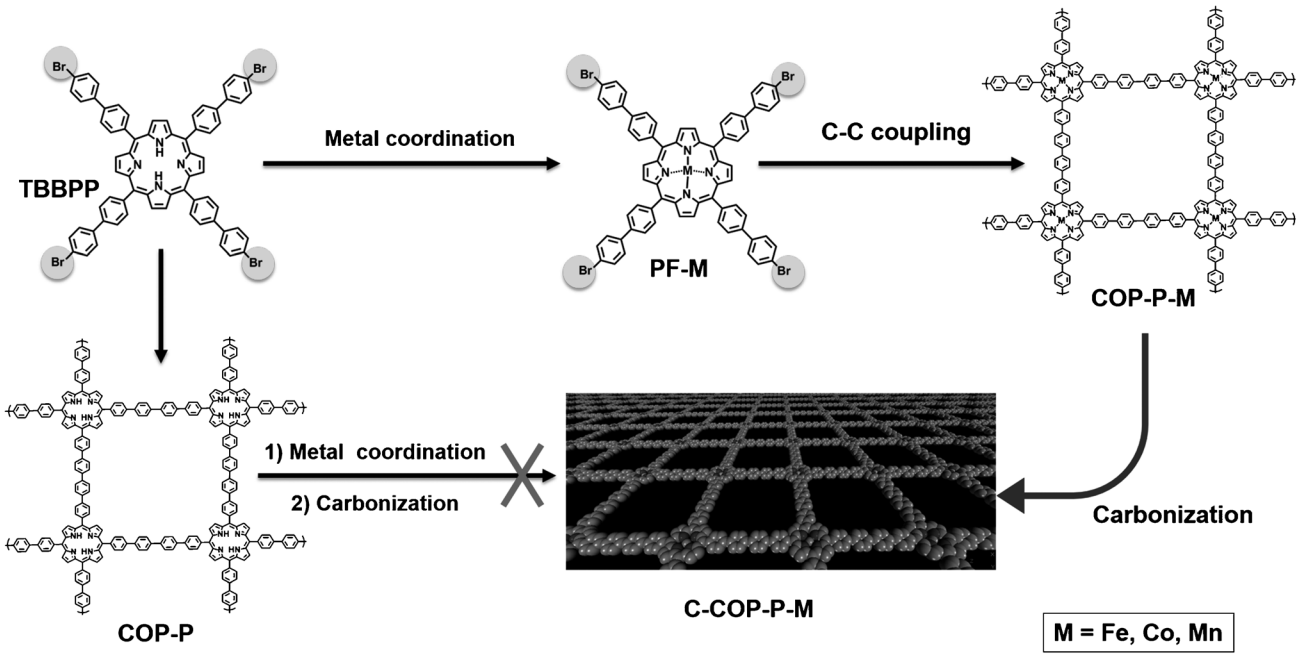

Scheme 1. The incorporation of non-precious metals (Fe, Co, or Mn) into C-COP in this work. Owing to the poor solubility of the synthesized COP materials in most common solvents, it is too difficult to introduce metals into the preformed COP-P.

the porphyrin ring at about 967 cm^{-1} in FTIR spectra for the metal-incorporated TBBPP (Supporting Information, Figure S4). Thereafter, the metal-incorporated COPs were produced by self-polycondensation of PF-M by heating the respective monomer, nickel(0) ($[Ni(cod)_2]$, 2,2′-bipyridyl, and bis(1,5-cyclooctadiene) in dehydrate DMF at 85 °C for overnight. For simplicity, we designated the resultant metal-incorporated COPs as COP-P-M (M = Fe, Co, Mn; P = porphyrin ring). The success of phenyl–phenyl coupling to produce COP-P-M was confirmed by the absence of the C–Br stretching peak at about 512 cm^{-1} in the FTIR spectra of the metal-incorporated COPs (Supporting Information, Figure S5–S7). Furthermore, ^{13}C/MAS NMR spectra indicate the skeletons of monomers (PF-M) were preserved in the COP-P-M (Figure 1a). Most transition metals incorporated in the porphyrin rings can be preserved even after washing with concentrated hydrochloric acid during the COP synthesis (Fe in COP-P-Fe: found, 4.95%, calculated, 5.74%; Co in COP-P-Co: found, 5.12%, calculated, 6.04%; Mn in COP-P-Mn: found, 4.85%, calculated, 5.65%).

The powder X-ray diffraction (XRD) patterns reveal no long-range crystallographic order for all of the three metal-incorporated COPs (Supporting Information, Figures S8–S10), which is presumably due to the distortion of phenyl rings that occurred during the polycondensation process.[7b,8] SEM images of COP-P-Fe (Figure 1b) and COP-P-Co (Supporting Information, Figure S11a,b) show the layer texture, suggesting the formation of graphene-like structures.

Subsequently, carbonization was performed to convert the COP-P-M into the metal-incorporated C-COP (designated as C-COP-P-M, M = Fe, Co, or Mn). The optimized carbonization temperature for C-COP-P-M was found to be 950 °C, as confirmed by the Raman spectra (Figure 1c) and electrocatalytic activities (described below). Figure 1c shows a strong G band, along with the single-peak 2D band, indicating a multilayered graphitic structure for all of the three C-COP-P-M samples. The relatively high intensity of the D band over the G band is attributable to the long-range disorder associated with those interdispersed small holes of rich edge defects (see below).[8] Unlike their metal-incorporated COP-P precursors, all of the three metal-incorporated C-COP-P-M samples showed XRD spectra with pronounced graphitic peaks (002) at 26° and (101) at 43° (Supporting Information, Figures S8–S10), indicating, once again, the formation of graphitic structures during carbonization. Transmission electron microscopic (TEM) images show porous texture in C-COP-P-Fe (Figure 1d,e). The corresponding elemental mapping on the TEM unit reveals that both carbon (Figure 1g) and metal, for example iron (Figure 1h) and cobalt (pink, Supporting Information, Figure S11f), atoms rather homogeneously dispersed over the C-COP-P skeletons. As expected, survey spectra from the X-ray photoelectron spectroscopic (XPS) measurements on all of the three C-COP-P-M (Supporting Information, Figure S12) shows characteristic peaks for the graphitic C around 284.7 eV, N centered at 398.5, and respective metal atoms. The high porosity of the C-COP-P-M facilitated physical adsorption of oxygen and/or water molecules, which are responsible for the O1s peaks seen in the Supporting Information, Figure S12.[2a] The corresponding high-resolution N1s peaks (Figure 1i; Supporting Information, Figure S12) show dominate components for the metal-bonded N and pyrrolic N atoms. This, together with FTIR spectra of the C-COP-P-M showing characteristic peaks for the porphyrin ring (Supporting Information, Figure S13), indicates once again that the porphyrin rings in the main skeletons of the COP-P-M precursors have been largely preserved even after the high temperature carbonization. TGA curves (Supporting

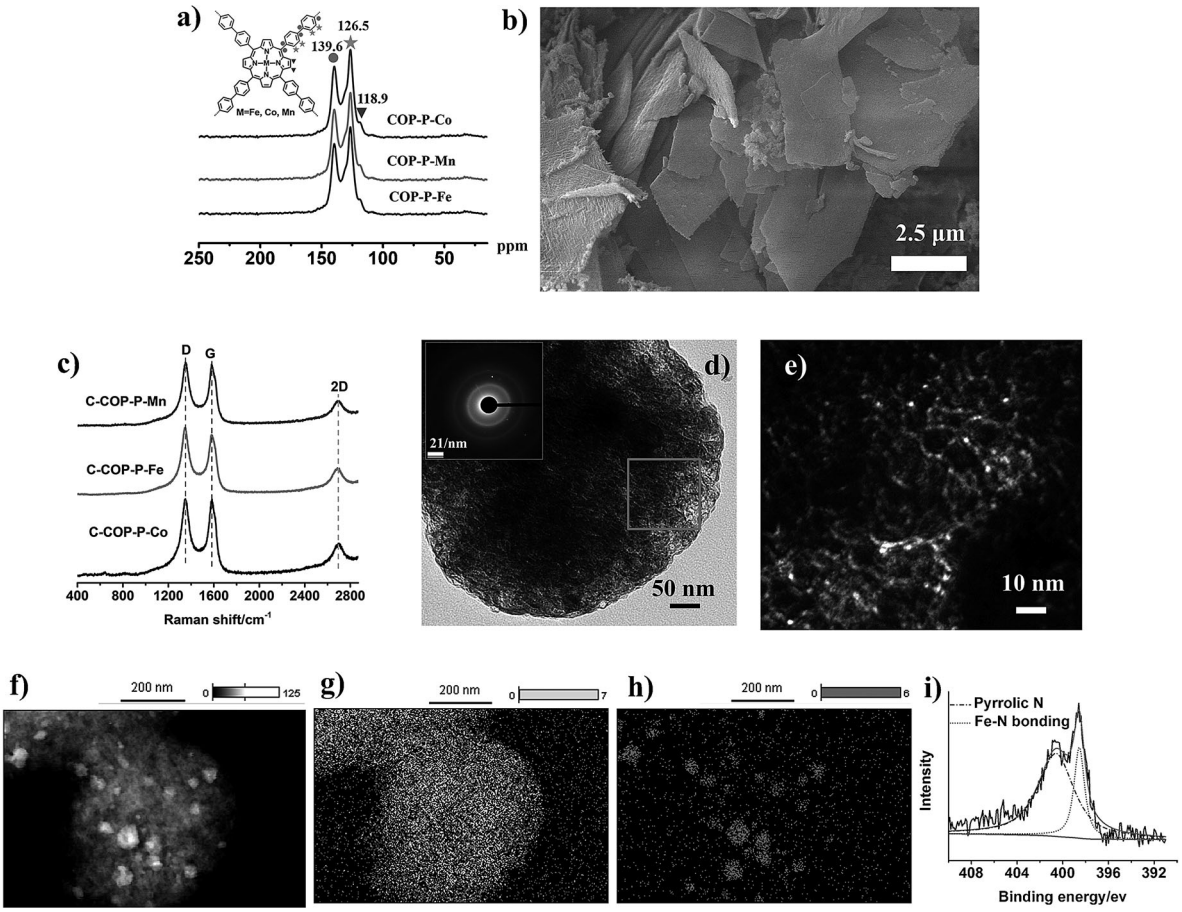

Figure 1. a) Solid-state ^{13}C NMR spectra of COP-P-M (M = Fe, Co, and Mn); b) SEM image of COP-P-Fe. c) Raman spectra of C-COP-P-M (M = Fe, Co, or Mn); d) TEM image of C-COP-P-Fe. Inset: the selected-area electron diffraction (SAED) pattern. e) An enlarged view of the area within the square in (d). f) TEM image of C-COP-P-Fe for element mapping. g) Carbon atom mapping of the C-COP-P-Fe sample. h) Iron atom mapping of the C-COP-P-Fe sample. i) XPS N 1s spectrum of the C-COP-P-Fe. The N 1s peak can be fitted with two Lorentzian peaks corresponding to Fe–N (398.7 eV) and pyrrolic N (400.6 eV), respectively.

Information, Figure S14) show that all of the three metal-incorporated C-COP-P-M samples possess a high thermodynamic stability with less than 20% weight loss even at 800 °C. These results suggest that C-COP-P-M could be a class of new electrocatalysts for ORR.

To evaluate the electrocatalytic activities for ORR, we first carried out cyclic voltammetric (CV) measurements on these newly synthesized metal-incorporated C-COP-P-M (M = Fe, Co, or Mn) samples, along with the C-COP-P and TBBPP with and without the metal complexation as reference. As shown in Figure 2a, all of the three metal-incorporated C-COP-P-M samples showed well-defined cathodic ORR peaks in aqueous solution of KOH (0.1M) saturated with O_2, but not N_2, within the potential range from 0.00 to 1.00 V. Comparing with the metal free C-COP-P (peak potential: ca. 0.49 V vs. RHE), the metal-incorporated C-COP-P-M electrocatalysts showed more positive ORR potentials with higher cathodic currents. In particular, peak potentials of the C-COP-P-Fe and C-COP-P-Co electrodes reached 0.77 V (vs. RHE) with about 60% increase in the cathodic current with respect to the metal-free C-COP-P samples (Figure 2a). However, the metal incorporation seems not to enhance the electrocatalytic performance for the TBBPP monomer (see below). Both the peak potential and cathodic current of the TBBPP electrode reduced from 0.56 V vs. RHE and 0.13 mA to 0.53 V vs. RHE and 0.06 mA, respectively, after metal complexation (Supporting Information, Figure S15).

The linear sweep voltammetric (LSV) curves (Supporting Information, Figure S16) for the C-COP-P-Fe electrocatalysts prepared at different carbonized temperatures, along with the metal free C-COP-P sample, the uncarbonized COP-P-Fe, and TBBPP electrode with and without the metal complexation, showed that carbonization significantly enhanced the electroactivity and that 950 °C is the best carbonization temperature in terms of the ORR performance (Supporting Information, Figure S16). This is because low-temperature carbonization cannot lead to a high graphitization degree to ensure a good conductivity, while high-temperature carbonization could destroy the conjugated structure of the C-COP-P frameworks with a concomitant reduce in conductivity. As such, we used 950 °C as the optimal temperature for carbonization of all of the COP-P samples for the ORR investigation in this study. The polycondensation polymerization of PF-M into COP-P-M seems to enhance both the ORR activity and stability for the metal-incorporated COPs, which after

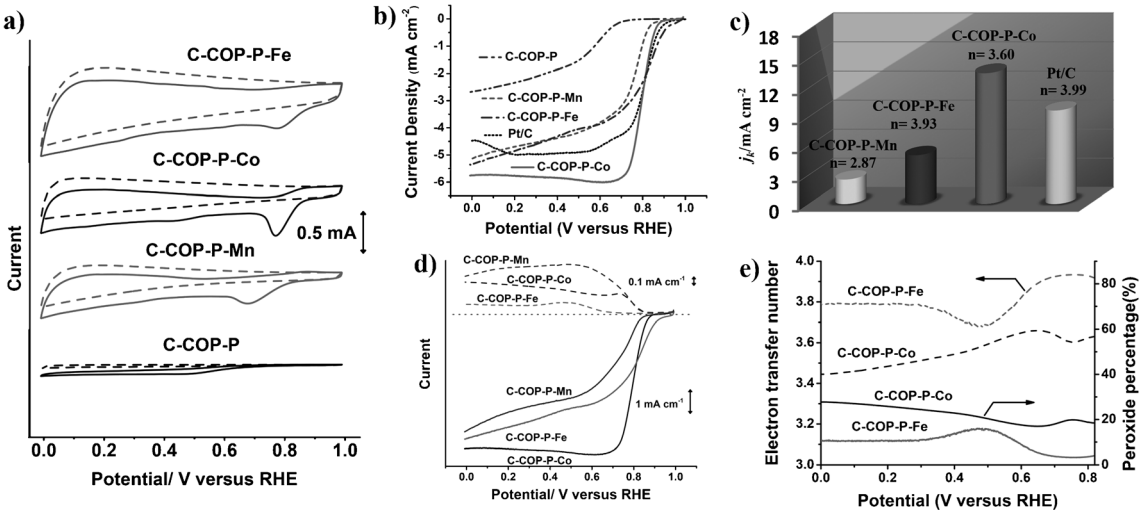

Figure 2. a) CV curves of the metal-incorporated and metal-free C-COP-P on glassy carbon electrodes in O_2-saturated (solid line) or N_2-saturated (dashed line) in 0.1 M KOH at a sweep rate of 10 mV s^{-1}. b) LSV curves of metal-incorporated C-COP-P-M in O_2-saturated 0.1 M KOH at 1600 rpm at a sweep rate of 5 mV s^{-1}. c) The comparison of electrochemical activity given as the kinetic-limiting current density (j_k) at 0.75 V (versus RHE) for the metal-incorporated C-COP-P-M. Also included are the calculated electron transfer numbers. d) Rotating ring-disk electrode (RRDE) voltammograms recorded with the metal-incorporated C-COP-P-M graphene in O_2-saturated 0.1 KOH at 1600 rpm. Disk current (I_d) (solid line) is shown on the lower half and the ring current (I_r) (dotted line) is shown on the upper half of the graph. The disk potential was scanned at 5 mV s^{-1} and the ring potential was constant at 1.5 V versus RHE. e) The calculated percentage of peroxide (solid line) and the electron transfer number (n) (dotted line) for the metal-incorporated C-COP-P-M (M = Fe, Co) samples at various potentials, derived from the corresponding RRDE data in (d). See the Supporting Information for detailed calculations.

carbonization could act as an efficient ORR catalyst even in acidic medium (see below).[9] Comparison of Figure 2a with Supporting Information, Figure S16 also reveals that metal incorporation improved the ORR performance of the COP-P materials after carbonization, but not for those without carbonization.

As seen in Figure 2b, all of the three metal-incorporated C-COP-P-M (M = Fe, Co, or Mn) electrodes exhibited remarkably enhanced electrocatalytic performance compared with the metal-free C-COP-P graphene. Among them, the C-COP-P-Fe electrode showed a similar onset potential as that of the commercially available Pt/C (0.98 V vs. RHE) (Figure 2b), while the C-COP-P-Co electrode exhibited a higher limited current than that of the benchmarked Pt/C (Figure 2b). The transferred electron number (n) per O_2 molecule for the C-COP-Fe and C-COP-P-Co electrodes were calculated from Koutecky–Levich (K-L) plots (Supporting Information, Figure S18 and S19) to be 3.81 and 3.56, respectively, at 0.35 V (compare Figure 2c,e), indicating a nearly 4e pathway for oxygen reduction. Furthermore, the kinetic limiting current densities (j_k) of C-COP-P-Co were derived from the K-L plots[4f] to be 13.50 mA cm^{-2} at 0.75 V (Figure S19), which are the highest values, outperforming the commercial Pt/C of 9 mA cm^{-2} at 0.75 V (Supporting Information, Figure S17), as shown in Figure 2c. The electron transfer number calculated from the rotating ring-disk electrode (RRDE) measurements (Figure 2d,e; Supporting Information, Figure S21) are similar as those derived from K-L plots (Supporting Information, Figures S18–S20), reconfirming the nearly 4e oxygen reduction process. It is worth noting that the calculated H_2O_2 yields are below 16% for the C-COP-P-Fe electrode and below 28% for the C-COP-P-Co electrode in the potential range of 0.00–0.80 V (Figure 2e; Supporting Information, Figure S22).

To investigate the methanol-crossover/CO-poisoning effects and durability, we carried out chronoamperometric measurements. As shown in Figure 3a, all of the three metal-incorporated C-COP-P-M electrodes were almost free from the methanol crossover effect. However, all of them showed weak CO-poisoning effect with about 10% current decrease upon the addition of CO (Figure 3b), compared to about 80% decrease for the Pt/C electrode under the same condition. The observed slight decrease in the ORR performance for the C-COP-P-M electrodes is probably due to adsorption of CO into the porous C-COP materials. Moreover, it was found that the C-COP-P-M electrodes exhibited a remarkably better long-term stability than the commercial Pt/C catalyst (Figure 3c).

Finally, we also investigated the ORR performance of the C-COP-P-Fe and C-COP-P-Co electrodes in O_2-saturated 0.1 M $HClO_4$ electrolyte. Like in alkaline media, the C-COP-P-Fe electrode showed a similar onset potential (ca. 0.89 V) as the Pt/C (ca. 0.96 V), while the C-COP-P-Co electrode exhibited a higher limited current than that of the Pt/C at the potential (less than about 0.26 V; Supporting Information, Figure S23). Overall, the C-COP-P-M electrode in the acid solution also showed a much better stability than the Pt/C electrode and free from the methanol crossover/CO-poisoning effects (Supporting Information, Figure S23 d–f), albeit a relatively poor ORR performance with respect to the alkaline medium. The transferred electron number (n) per O_2 molecule for the C-COP-P-Fe and C-COP-P-Co electrodes in the acidic medium calculated by the K-L equation is 3.82 and 3.61 (Supporting Information, Figure S24 and S25) at 0.35–0.45 V (Supporting Information, Figure S23c), in a good

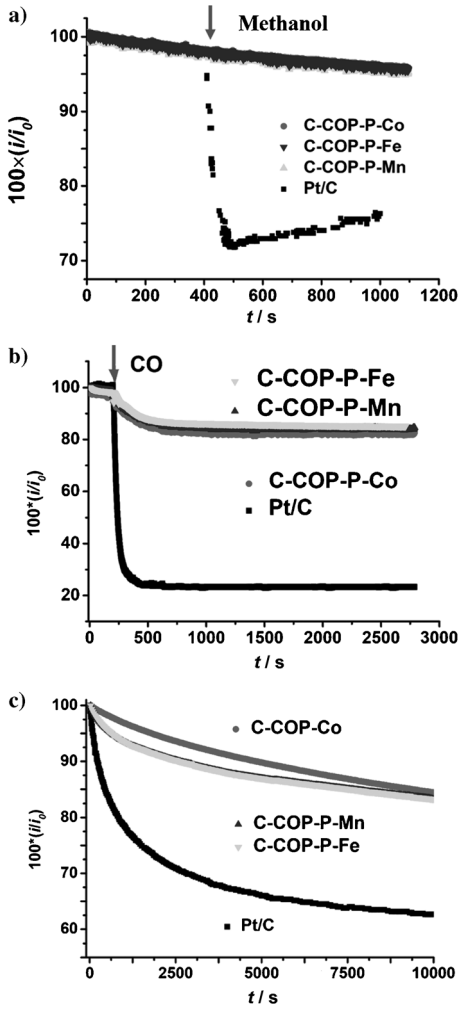

Figure 3. a) Methanol-crossover and b) CO-poison effects. c) Durability evaluation from the *i*–*t* chronoamperometric responses of the metal-incorporated C-COP electrodes in aqueous solution of KOH (0.1 M) saturated with O_2. Also included is the commercial Pt/C electrode for comparison. The arrows indicate the addition of 3 mL methanol into the O_2-saturated electrochemical cell after about 400 s in (a) and the addition of 55 mL min^{-1} CO gas into the electrochemical cell saturated by 550 mL min^{-1} O_2 flow for 200 s (b).

agreement with those calculated by the RRDE curves (Supporting Information, Figure S23b), suggesting a nearly 4e ORR pathway even in the acid solution. The calculated yields of H_2O_2 for the C-COP-P-Fe and C-COP-P-Co electrodes are less than 19% and 35%, respectively (Supporting Information, Figure S23c) under the potential range of 0.0–0.6 V.

In summary, we have developed a class of new efficient electrocatalysts for oxygen reduction in both alkaline and acidic media by synthesizing 2D covalent organic polymers (COPs) with precisely-controlled locations of nitrogen heteroatoms and pore sizes, followed by complexation with metal (such as Fe, Co, and Mn) and carbonization of the metal-incorporated COPs into C-COP materials. The resultant metal-incorporated C-COP materials were found to show efficient electrocatalytic activities toward 4e oxygen reduction in both alkaline and acid media with an excellent stability and free from any methanol-crossover/CO-poisoning effects. Clearly, therefore, these newly-developed metal-incorporated C-COP materials hold great potential as efficient ORR catalysts for fuel cells. This work opens up an avenue for the rational design and development of novel highly-efficient ORR electrocatalysts from various 2D covalent organic polymer and metal complexes.

Received: October 12, 2013
Revised: December 20, 2013
Published online: January 29, 2014

Keywords: covalent organic polymers · electrocatalysts · graphene analogues · metal–organic frameworks · oxygen reduction reaction

[1] a) Z. Chen, M. Waje, W. Li, Y. Yan, *Angew. Chem.* **2007**, *119*, 4138–4141; *Angew. Chem. Int. Ed.* **2007**, *46*, 4060–4063; b) H. A. Gasteiger, S. S. Kocha, B. Sompalli, F. T. Wagner, *Appl. Catal. B* **2005**, *56*, 9–35.

[2] a) Z. Chen, D. Higgins, A. Yu, L. Zhang, J. Zhang, *Energy Environ. Sci.* **2011**, *4*, 3167–3192; b) M. Lefèvre, E. Proietti, F. Jaouen, J.-P. Dodelet, *Science* **2009**, *324*, 71–74; c) R. Liu, C. von Malotki, L. Arnold, N. Koshino, H. Higashimura, M. Baumgarten, K. Mullen, *J. Am. Chem. Soc.* **2011**, *133*, 10372–10375; d) Y. Liang, Y. Li, H. Wang, J. Zhou, J. Wang, T. Regier, H. Dai, *Nat. Mater.* **2011**, *10*, 780–786; e) R. Jasinski, *Nature* **1964**, *201*, 1212–1213.

[3] H. Alt, H. Binder, G. Sandstede, *J. Catal.* **1973**, *28*, 8–19.

[4] a) L. Qu, Y. Liu, J.-B. Baek, L. Dai, *ACS Nano* **2010**, *4*, 1321–1326; b) L. Dai, D. W. Chang, J.-B. Baek, W. Lu, *Small* **2012**, *8*, 1130–1166; c) L. Qu, L. Dai, M. Stone, Z. Xia, Z. L. Wang, *Science* **2008**, *322*, 238–242; d) L. Y. Feng, Y. Y. Yan, Y. G. Chen, L. J. Wang, *Energy Environ. Sci.* **2011**, *4*, 1892–1899; e) S. Y. Wang, D. S. Yu, L. M. Dai, *J. Am. Chem. Soc.* **2011**, *133*, 5182–5185; f) S. Y. Wang, D. S. Yu, L. M. Dai, D. W. Chang, J. B. Baek, *ACS Nano* **2011**, *5*, 6202–6209; g) Y. Zheng, Y. Jiao, J. Chen, J. Liu, J. Liang, A. Du, W. M. Zhang, Z. H. Zhu, S. C. Smith, M. Jaroniec, G. Q. Lu, S. Z. Qiao, *J. Am. Chem. Soc.* **2011**, *133*, 20116–20119; h) L. Yang, S. Jiang, Y. Zhao, L. Zhu, S. Chen, X. Wang, W. Qiang, J. Ma, Y. Ma, Z. Hu, *Angew. Chem.* **2011**, *123*, 7270–7273; *Angew. Chem. Int. Ed.* **2011**, *50*, 7132–7135; i) Y. Zheng, J. Liu, J, Liang, M. Jaronic, S. Z. Qiao, *Energy Environ. Sci.* **2012**, *5*, 6717–6731; j) X. Wang, J. S. Lee, Q. Zhu, J. Liu, Y. Wang, S. Dai, *Chem. Mater.* **2010**, *22*, 2178–2180; k) D. Yu, E. Nagelli, F. Du, L. Dai, *J. Phys. Chem. Lett.* **2010**, *1*, 2165–2173; l) L. Dai, *Acc. Chem. Res.* **2013**, *46*, 31–42.

[5] K. P. Gong, F. Du, Z. H. Xia, M. Durstock, L. M. Dai, *Science* **2009**, *323*, 760–764.

[6] R. Liu, D. Wu, X. Feng, K. Müllen, *Angew. Chem.* **2010**, *122*, 2619–2623; *Angew. Chem. Int. Ed.* **2010**, *49*, 2565–2569.

[7] a) Z. H. Xiang, D. P. Cao, *J. Mater. Chem. A* **2013**, *1*, 2691–2718; b) Z. H. Xiang, D. P. Cao, *Macromol. Rapid Commun.* **2012**, *33*, 1184–1190; c) Z. H. Xiang, D. P. Cao, W. C. Wang, W. T. Yang, B. Y. Han, J. M. Lu, *J. Phys. Chem. C* **2012**, *116*, 5974–5980; d) Z. H. Xiang, X. Zhou, C. H. Zhou, S. Zhong, X. He, C. P. Qin, D. P. Cao, *J. Mater. Chem.* **2012**, *22*, 22663–22669.

[8] T. Ben, K. Shi, Y. Cui, C. Pei, Y. Zuo, H. Guo, D. Zhang, J. Xu, F. Deng, Z. Tian, S. Qiu, *J. Mater. Chem.* **2011**, *21*, 18208–18214.

[9] a) J. Tang, T. Wang, X. Pan, X. Sun, X. Fan, Y. Guo, H. Xue, J. He, *J. Phys. Chem. C* **2013**, *117*, 16896–16906; b) F. J. Maldonado-Hódar, C. Moreno-Castilla, J. Rivera-Utrilla, Y. Hanzawa, Y. Yamada, *Langmuir* **2000**, *16*, 4367–4373; c) G. Wu, P. Zelenay, *Acc. Chem. Res.* **2013**, *46*, 1878–1889.

